

AD

AD-E403 065

Technical Report ARAET-TR-05013

## SHAPED CHARGE JET FLASH RADIOGRAPH DIGITIZATION

James D. Pham  
Ernest L. Baker  
Stanley DeFisher

September 2005



U.S. ARMY ARMAMENT RESEARCH, DEVELOPMENT AND  
ENGINEERING CENTER

Armaments Engineering & Technology Center

Picatinny, New Jersey

Approved for public release; distribution is unlimited.

The views, opinions, and/or findings contained in this report are those of the author(s) and should not be construed as an official Department of the Army position, policy, or decision, unless so designated by other documentation.

The citation in this report of the names of commercial firms or commercially available products or services does not constitute official endorsement by or approval of the U.S. Government.

Destroy this report when no longer needed by any method that will prevent disclosure of its contents or reconstruction of the document. Do not return to the originator.

REPORT DOCUMENTATION PAGE

Form Approved  
OMB No. 0704-01-0188

The public reporting burden for this collection of information is estimated to average 1 hour per response, including the time for reviewing instructions, searching existing data sources, gathering and maintaining the data needed, and completing and reviewing the collection of information. Send comments regarding this burden estimate or any other aspect of this collection of information, including suggestions for reducing the burden to Department of Defense, Washington Headquarters Services Directorate for Information Operations and Reports (0704-0188), 1215 Jefferson Davis Highway, Suite 1204, Arlington, VA 22202-4302. Respondents should be aware that notwithstanding any other provision of law, no person shall be subject to any penalty for failing to comply with a collection of information if it does not display a currently valid OMB control number.  
PLEASE DO NOT RETURN YOUR FORM TO THE ABOVE ADDRESS.

1. REPORT DATE (DD-MM-YYYY) **September 2005**      2. REPORT TYPE      3. DATES COVERED (From - To)

4. TITLE AND SUBTITLE  
**Shaped Charge Jet Flash Radiograph Digitization**

5a. CONTRACT NUMBER  
5b. GRANT NUMBER  
5c. PROGRAM ELEMENT NUMBER

6. AUTHORS  
**James D. Pham, Ernest L. Baker, and Stanley DeFisher**

5d. PROJECT NUMBER  
5e. TASK NUMBER  
5f. WORK UNIT NUMBER

7. PERFORMING ORGANIZATION NAME(S) AND ADDRESS(ES)  
**U.S. Army ARDEC, AETC  
Energetics, Warheads & Environmental Technology  
(AMSRD-AAR-AEE-W)  
Picatinny, NJ 07806-5000**

8. PERFORMING ORGANIZATION REPORT NUMBER

9. SPONSORING/MONITORING AGENCY NAME(S) AND ADDRESS(ES)  
**U.S. Army ARDEC, EM  
Technical Research Center (AMSRD-AAR-EMK)  
Picatinny, NJ 07806-5000**

10. SPONSOR/MONITOR'S ACRONYM(S)  
11. SPONSOR/MONITOR'S REPORT NUMBER(S)  
**Technical Report ARAET-TR-05013**

12. DISTRIBUTION/AVAILABILITY STATEMENT  
**Approved for public release; distribution is unlimited.**

13. SUPPLEMENTARY NOTES

14. ABSTRACT  
The flash radiograph digitization of shaped chare jets provides warhead designers with the data required for empirically based models, as well as the jet characterization used for comparison with high rate continuum modeling. Reduced digitization results include jet tip velocity, jet accumulated length, accumulated mass, accumulated energy, break up time, maximum and average jet diameters, and the ductility factor (Q). This computer program provides a systematic method of characterizing a shaped charge warhead by means of quantifying the shaped charge jet parameters. The break up time, for instance, shows when the shaped charge jet particulates. This parameter is essential for shaped charge performance, because it relates to how deep the penetration is, since the penetration is decreased significantly once the jet particulates. The Q ductility factor is another example of the characterization of the jet. In general, the higher the number Q (more ductile), more penetration is expected. The accumulated mass and break up time from the digitization computations can be used in penetration simulation prediction.

15. SUBJECT TERMS  
**Digitization      Flash radiograph      Shaped charge jet      Jet characterization      Breakup time**

16. SECURITY CLASSIFICATION OF:			17. LIMITATION OF ABSTRACT  <b>SAR</b>	18. NUMBER OF PAGES  <b>44</b>	19a. NAME OF RESPONSIBLE PERSON <b>J. Pham, E. Baker, and S. DeFisher</b>
a. REPORT <b>U</b>	b. ABSTRACT <b>U</b>	c. THIS PAGE <b>U</b>			19b. TELEPHONE NUMBER (Include area code) <b>(973) 724-4818</b>

## CONTENTS

	Page
Introduction	1
Digitization for Flash Radiographs of Shaped Charge Jet	1
Naming and Numbering Convention	2
Film Digitization	2
Interpolation and Extrapolation	2
Films Longer than Digitizer Tablet	2
Hardware	3
Computer Code	3
Input Parameters	3
Output Parameters	5
Calculation	5
Discussions	12
Assumptions	19
Comparison to the 2-D CALE Hydrocode	19
Conclusions	20
Appendix - Output from Program No. 1, Input to Program No. 2	21
References	39
Distribution List	41

## FIGURES

1	Typical x-ray of a shaped charge jet	1
2	Digitizing scheme of jet particles	2
3	Long film on digitizing tablet	3
4	Input screen	4
5	Accumulated length versus velocity	7
6	Accumulated mass versus velocity	8
7	Volume calculation	9

FIGURES  
(continued)

	Page
8 Accumulated energy versus velocity	10
9 Breakup time versus velocity	10
10 Q versus velocity	11
11 Accumulated mass versus velocity from shaped charge digitization code and 2-D CALE hydrocode	19

TABLES

1 Digitization output	12
2 Average $\bar{Q}$ values for copper lined devices	16
3 Average $\bar{Q}$ values for molybdenum lined devices	17
4 Average $\bar{Q}$ values for tungsten lined devices	17
5 Average $t_b / D$ values for copper lined devices	17
6 Average $t_b / D$ values for molybdenum lined devices	18
7 Average $t_b / D$ values for tungsten lined devices	19

## INTRODUCTION

Although shaped charge jet mass and momentum characteristics can be accurately simulated and tailored using high rate continuum modeling, the subsequent break-up of a shaped charge jet is currently simulated using empirically based models. These models are used to predict jet break-up time, jet length, and jet penetration capability. Shaped charge warheads are designed using the hydrocode simulation and subsequently tested, and flash radiographs of the shaped charge are obtained. Flash radiograph data are essential to shaped charge design for determination of the jet characteristics, which are not readily available from the hydrocode simulation results. In order to quantify the results of these warheads, the flash radiograph digitization of shaped charge jets are done to provide warhead designers with the data required for these empirically based models. The quantified results of the jet characterization are also used for comparison with high rate continuum modeling performed during warhead design optimization with different liner contours, explosives, and liner materials.

### DIGITIZATION FOR FLASH RADIOGRAPHS OF SHAPED CHARGE JET

Since a shaped charge jet tip goes faster than its rear, the jet stretches and eventually breaks up. Typically, shaped charge jet radiographs are taken at least 20 charge diameter distance to allow time for the jet to break up. Flash radiographs are normally taken so that the tip of the jet is captured in the earliest time, and the particles with velocities around 3 km/s were captured in the latest film. Other flash radiographs are taken between these times to capture the middle part of the jet. The jet images are laid on the digitized tablet and the entire jet is digitized. Typical flash x-rays are shown in figure 1.

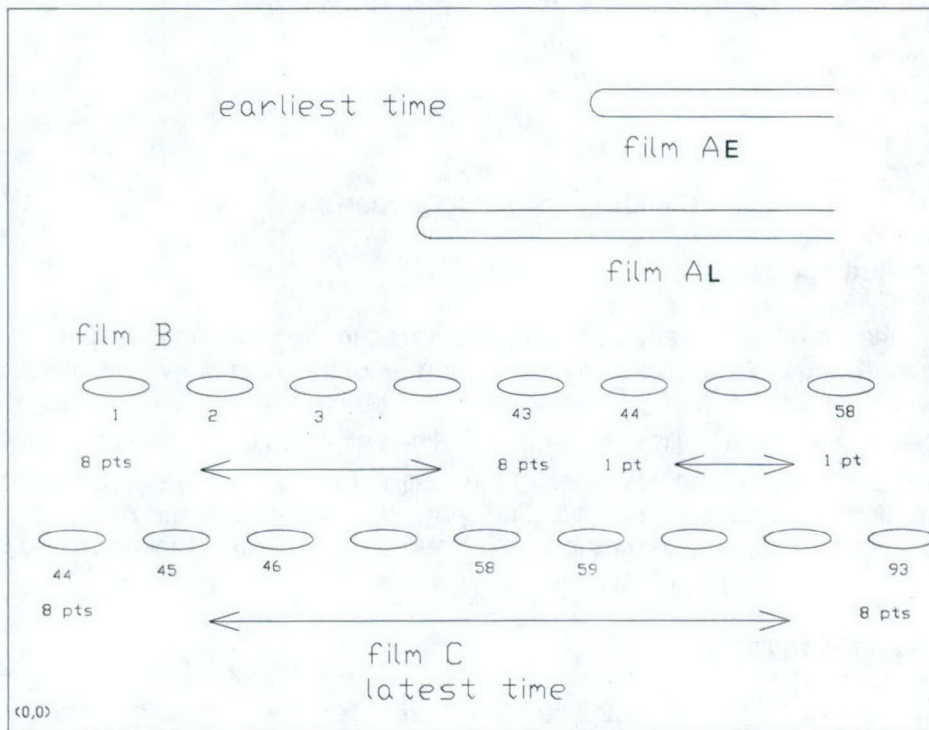


Figure 1  
Typical x-ray of a shaped charge jet

## Naming and Numbering Convention

Films are named from the earliest to the latest times:  $A_E$ ,  $A_L$ , B, and C. The tip particle is numbered as 1 and continued to the end of the jet.

## Film Digitization

Using the typical films as shown in figure 1, the digitization scheme is as follows:

- Particles 1 to 43 in film B are digitized for eight points for each particle. From particles 44 to 58, only 1 point is digitized (fig. 2).
- In film C, eight points for each particle are digitized for all particles from 44 to 93.
- In film  $A_E$  and  $A_L$ , only the tips (one point each) are digitized.

Note that the eight point/one point digitization scheme is done to reduce the digitization time. Alternately, eight points can be taken for every particle in films B and C and the average values can be taken.

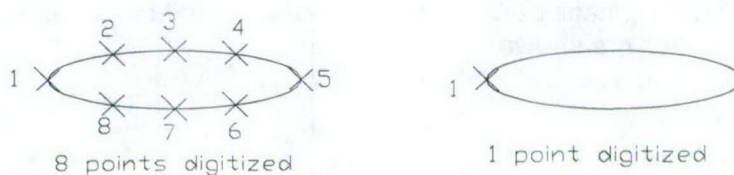


Figure 2  
Digitizing scheme of jet particles

## Interpolation and Extrapolation

A shaped charge jet is typically very long compared to the x-ray films, especially in larger shaped charge warheads. Therefore, only the tip portion of the jet is shown on film B and the rear portion is on film C, with a few common particles in both films. In this example, the velocity of the tip was determined by the films  $A_E$  and  $A_L$ . The velocities of particles 44 to 58 are also known from films B and C, but the velocities of the rest of the particles are determined by the interpolation (particles 2 to 43) and extrapolation (particles 59 to 93) based on their positions. Both interpolation and extrapolation methods are fitted to the first order equation and based on the virtual origin theory (ref. 1).

## Films Longer Than the Digitized Tablet

Some films are longer than the digitized tablet. In this case, the computer code asks for the references A and B. The film is then slid to the left, until point B coincides with point A, and digitized until the end of the film (figure 3). This allows for film digitization of longer than the tablet. The code will automatically keep track of the references and update the new positions of the jet particles.

The code will automatically keep track of the references and update the new positions of the jet particles.

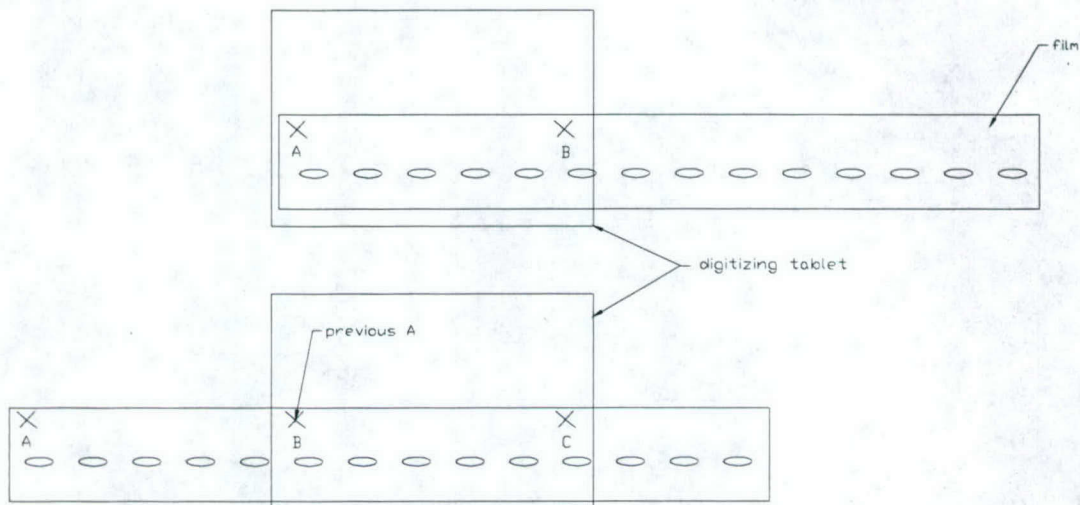


Figure 3  
Long film on digitizing tablet

## HARDWARE

The films are digitized using CALCOMP model 9500 digitizing tablet. It has the resolution of  $0.25 \times 10^{-3}$  in., accuracy of  $\pm 0.003$  in. and about 6 ft in length. The digitized tablet is connected to a computer via a serial com port. Films are placed and taped in place. A digital input device was placed on the film and manually recorded the data.

## COMPUTER CODE

The digitization code consists of two programs. Both were written in VISUAL BASIC, version 6. The first program digitizes the jet radiographs into x, y coordinates and the references, and writes these data to an output file named AP\_FILE.TXT. The sample file is included in the appendix. The second program reads this file in addition to the input entered in figure 4 and calculates the jet parameters.

### Input Parameters

Input parameters are required to be filled in as shown in figure 4.

- X-ray: Enter x-ray number (information purpose)



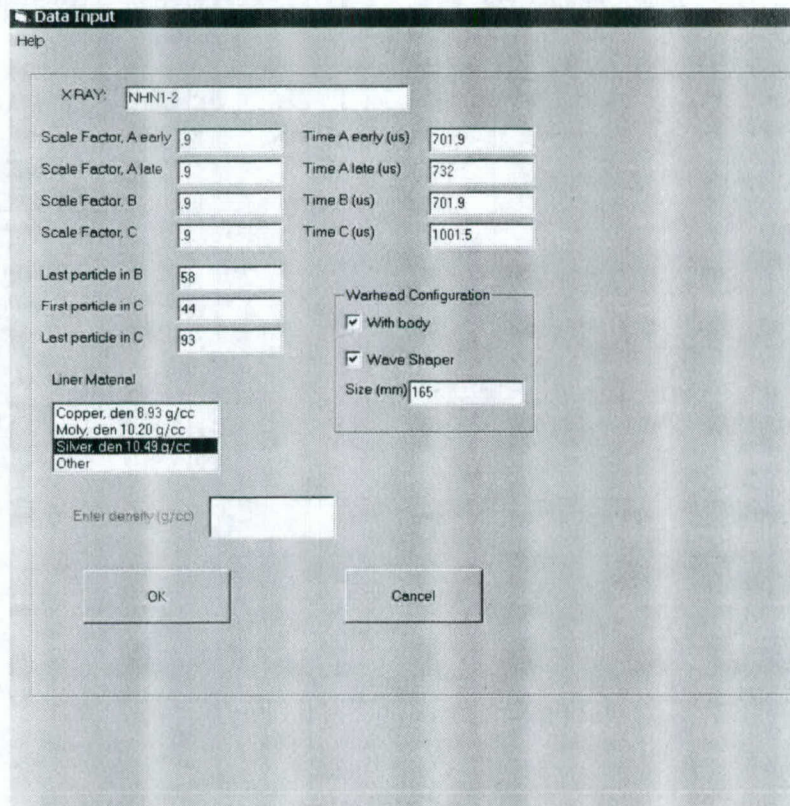


Figure 4  
Input screen

- Scale factors  $A_E$ ,  $A_L$ , B, and C: Images on the x-ray films are larger than the particles. Therefore, the measurements are adjusted to the scale factor. A rod with knots with known distance is placed in the shot line and an image taken prior to detonating the warhead. Scale factor of film B, for example, is equal

$$SF_B = \frac{disRod}{disMeasured}$$

where

disRod is the known distance on rod, usually 50 mm  
disMeasured is the measured distance on x-ray B

- Last particle in B, first particle in C, last particle in C: In this example, they are 58, 44, 93, respectively.
- Liner material: Liner material is chosen by selecting in the menu, or it can be chosen as "other", in which case, density in  $g/cm^3$  is entered in the box.
- Time  $A_E$ ,  $A_L$ , B, C: Enter times of  $A_E$ ,  $A_L$ , B, and C films.

- Warhead configuration: This is for informational purposes only. Click on the appropriate boxes and enter the size of the warhead.

### Output Parameters

The code provides both tabulated tables of particle angles, maximum and average jet diameters, velocities, accumulated mass, accumulated length, accumulated energy, break up times, ductility factor numbers (Q), average breakup time, average Q factor as well as plots of accumulated length versus velocity, accumulated mass versus velocity, accumulated energy versus velocity, Q versus velocity, and breakup time versus velocity.

### Calculation

#### Nomenclatures

$A_E$	=	x coordinate of early A film
$A_L$	=	x coordinate of late A film
$V_T$	=	Jet tip velocity
$\bar{t}_b$	=	Average break up time ( $\mu\text{s}$ )
$t_b(V)$	=	Breakup time as a function of V
$SF_{A_E}$	=	Scaled factor of early film in A
$SF_{A_L}$	=	Scaled factor of late film in A
$SF_B$	=	Scaled factor of film B
$SF_C$	=	Scaled factor of film C
$\sum L$	=	Accumulated jet length (cm)
$\sum M$	=	Accumulated jet mass (g)
$\sum E$	=	Accumulated energy (KJ)
$L(V)$	=	Accumulated jet length as a function of V
$M(V)$	=	Accumulated jet mass as a function of V
$L_p$	=	length of a jet particle = $x_5 - x_1$
$M_p$	=	mass of a jet particle
$E_p$	=	energy of a jet particle
$\Delta V$	=	Difference of tip and tail velocity (cm/ $\mu\text{s}$ )
$\bar{Q}$	=	Average ductility number ( $\text{cm}^{1/3} \mu\text{s}^{1/3} \text{g}^{1/3}$ )
$Q(V)$	=	Instantaneous ductility number as a function of V
$\alpha$	=	angle of jet particle (deg)
$\rho$	=	density ( $\text{g}/\text{cm}^3$ )
Vol	=	Volume of a jet particle ( $\text{cm}^3$ )
$\bar{\phi}$	=	average jet particle diameter
$\phi_{\text{max}}$	=	maximum jet particle diameter
$x_5$	=	x coordinate of point 5 of a particle

- $x_1$  = x coordinate of point 1 of a particle
- $y_1$  = y coordinate of point 1 of a particle
- $y_5$  = y coordinate of point 5 of a particle

### Jet Velocity

Jet velocity of the tip ( $V_T$ ) is calculated by taking the coordinates of the tips in films  $A_E$  and  $A_L$ .

$$V_T = \frac{A_E SF_{A_E} - A_L SF_{A_L}}{t_L - t_E}$$

Since there is no information available for particles 2 to 43 to calculate the velocities for these particles, the velocities are interpolated based on the known positions of these tips. In this example, particles 1 and 44 to 58, in film B, are used to find the position as a function of velocity. A first order fit is used to find the missing velocities based on their positions. Similarly, velocities of particles 59 to 93 are extrapolated using the function fitted by particles 44 to 58 based on film C.

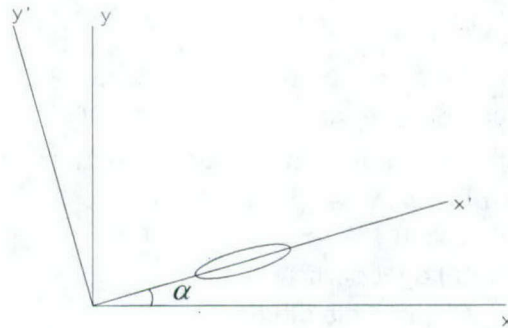
### Axes Transformation

Since many particle orientations in a shaped charge jet are not lined up with the digitizer axis, axis transformation is used such that

$$\begin{aligned} x' &= x \cos \alpha + y \sin \alpha \\ y' &= y \cos \alpha - x \sin \alpha \end{aligned}$$

where

$$\alpha = \tan^{-1} \left( \frac{y_5 - y_1}{x_5 - x_1} \right)$$



The particle lengths and mass use the transformed axis.

### Accumulated Length versus Velocity (fig. 5)

Accumulated length is calculated for breakup time. Lengths of particles 1 to 43, in film B in figure 1, are added by taking the difference of x coordinates of point 5 and point 1 of each particle (the other points are used subsequently for volume calculation). The same scheme is applied for film C where lengths of particles 44 to 93 are added to the previous accumulated length in film B.

$$\sum L = \sum_{\text{particle 1}}^{\text{particle 43}} L_p + \sum_{\text{particle 44}}^{\text{particle 93}} L_p$$

Film B    Film C

The accumulated length is then fitted to the second order with the velocity.

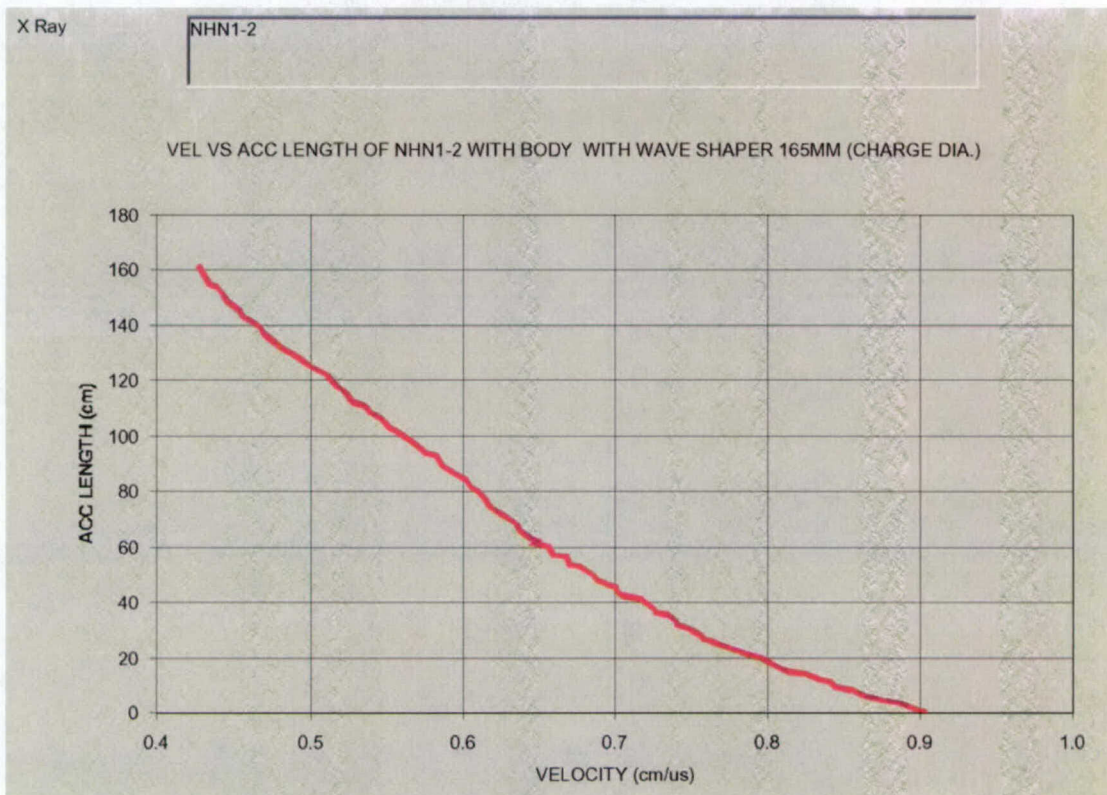


Figure 5  
Accumulated length versus velocity

### Accumulated Mass versus Velocity (fig. 6)

Jet mass is also calculated to find the kinetic energy of the jet for the penetration calculation.

Volumes of particles 1 to 43 in film B in figure 1 are added by taking the x and y coordinates of points 1 through 8 of each particle. The same scheme is applied for film C where volumes of particles 44 to 93 are added to the previous accumulated volume.

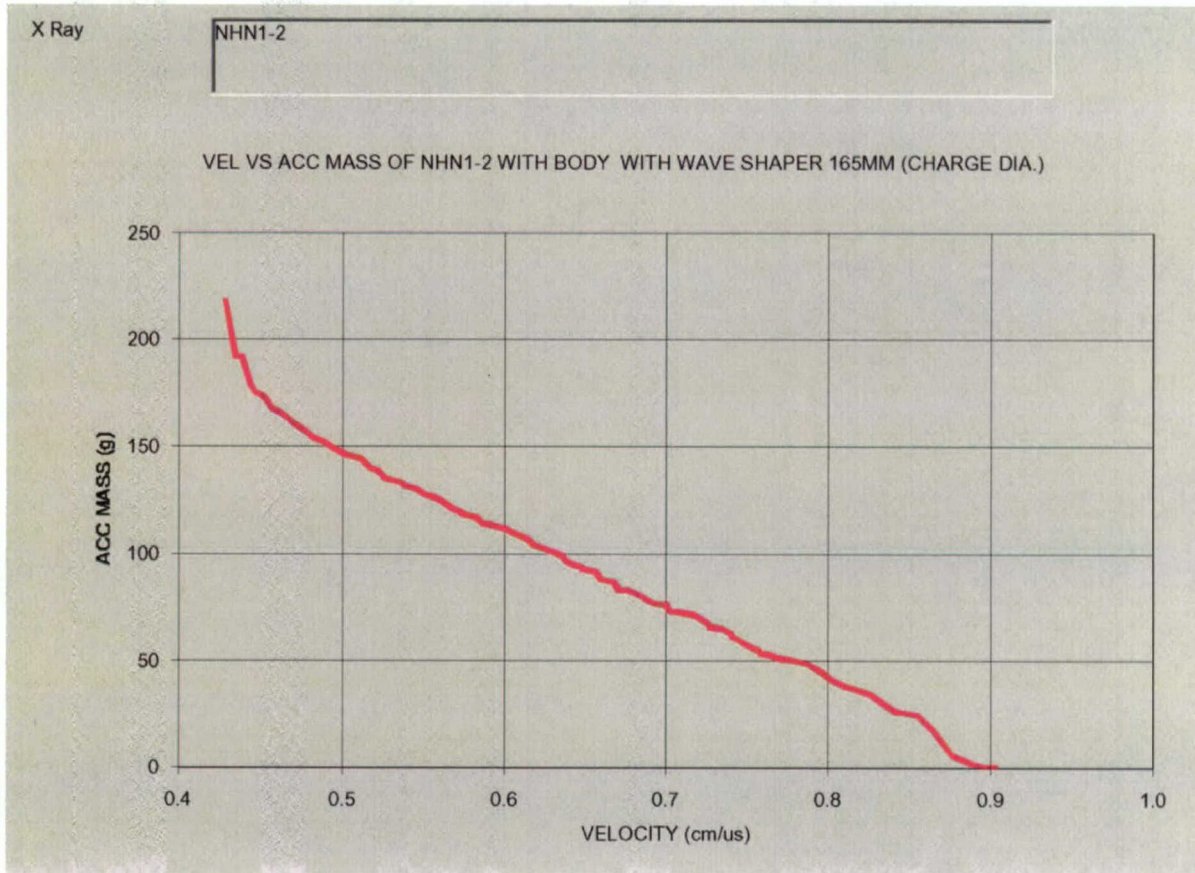


Figure 6  
Accumulated mass versus velocity

Assuming the round cross section, the volume of a particle is calculated based on the eight points digitized. The top curve [ $f_1(x)$ ], is composed of five points, from 1 to 5, and the bottom curve [ $f_2(x)$ ], is also composed of five points with point 1 and 5 as in the top curve and points 6, 7, and 8 (fig. 7) as the bottom curve. These curves are fitted to the second order equations, where  $f_1(x) = a_1x^2 + b_1x + c_1$  and  $f_2(x) = a_2x^2 + b_2x + c_2$ . Let

$$\Delta A = a_1 - a_2, \Delta B = b_1 - b_2, \Delta C = c_1 - c_2$$

$$Vol = \int_{x_1}^{x_5} \frac{\pi}{4} (\Delta Ax^2 + \Delta Bx + \Delta C)^2 dx$$

$$= \frac{\pi}{4} \left[ \frac{\Delta A^2}{5} x^5 + \frac{\Delta A \Delta B}{2} x^4 + \frac{2\Delta A \Delta C + \Delta B^2}{3} x^3 + \Delta B \Delta C x^2 + \Delta C^2 x \right]_{x_1}^{x_5}$$

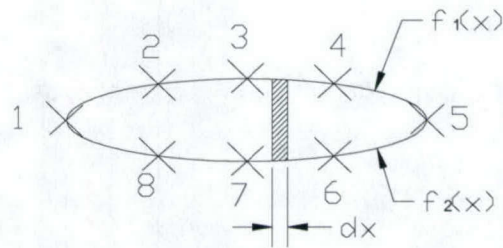


Figure 7  
Volume calculation

and

$$M_p = \rho Vol$$

$$\sum M = \sum_{particle1}^{particle43} M_p + \sum_{particle44}^{particle93} M_p$$

Film B    Film C

The accumulated mass is then fitted to the second order with the velocity to find  $M(V)$  for subsequent calculations.

**Accumulated Energy versus Velocity (fig. 8)**

$$\sum E = \sum_{particle1}^{particle43} \frac{1}{2} M_p V^2 + \sum_{particle44}^{particle93} \frac{1}{2} M_p V^2$$

Film B                      Film C

**Break Up Time versus Velocity (fig. 9)**

Average breakup time and instantaneous breakup time are calculated based on the accumulated length. Breakup time predicts the jet penetration performance because penetration performance is reduced if the jet breaks up too early.

Average and instantaneous breakup times are estimated below

$$\bar{t}_b = \frac{\sum L}{\Delta V}$$

$$t_b(V) = \frac{dL}{dV}$$

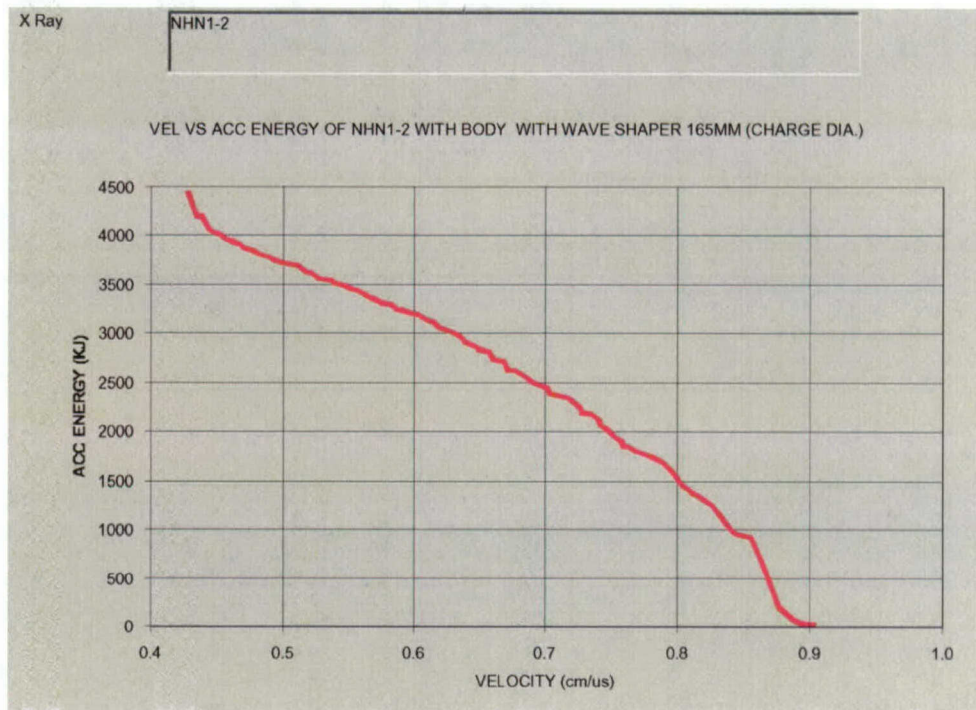


Figure 8  
Accumulated energy versus velocity

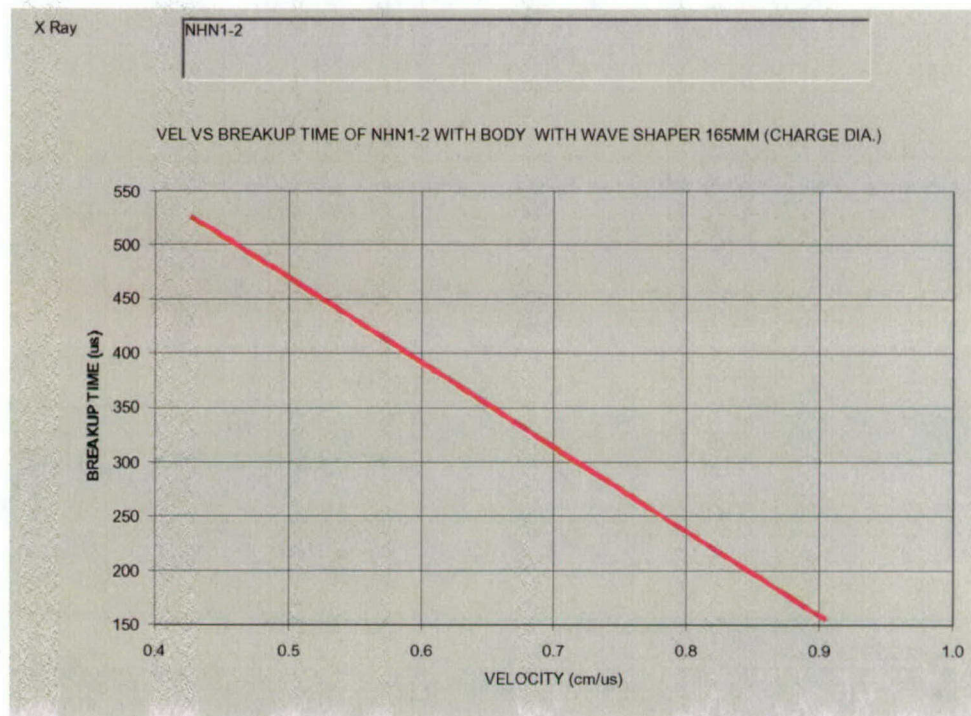


Figure 9  
Breakup time versus velocity

### Jet Ductility Number Q (fig. 10)

Both average jet ductility and instantaneous numbers are estimated next. The ductility number is of great interest because it shows the correlation of the jet performance with increased Q number. Reference 2 shows the relationship

$$\bar{Q} = t_b \left( \frac{\pi \Delta V}{\sum M_p} \right)^{1/3}$$

$$Q(V) = t_b \left( \frac{1}{\pi} \frac{dM}{dV} \right)^{-1/3}$$

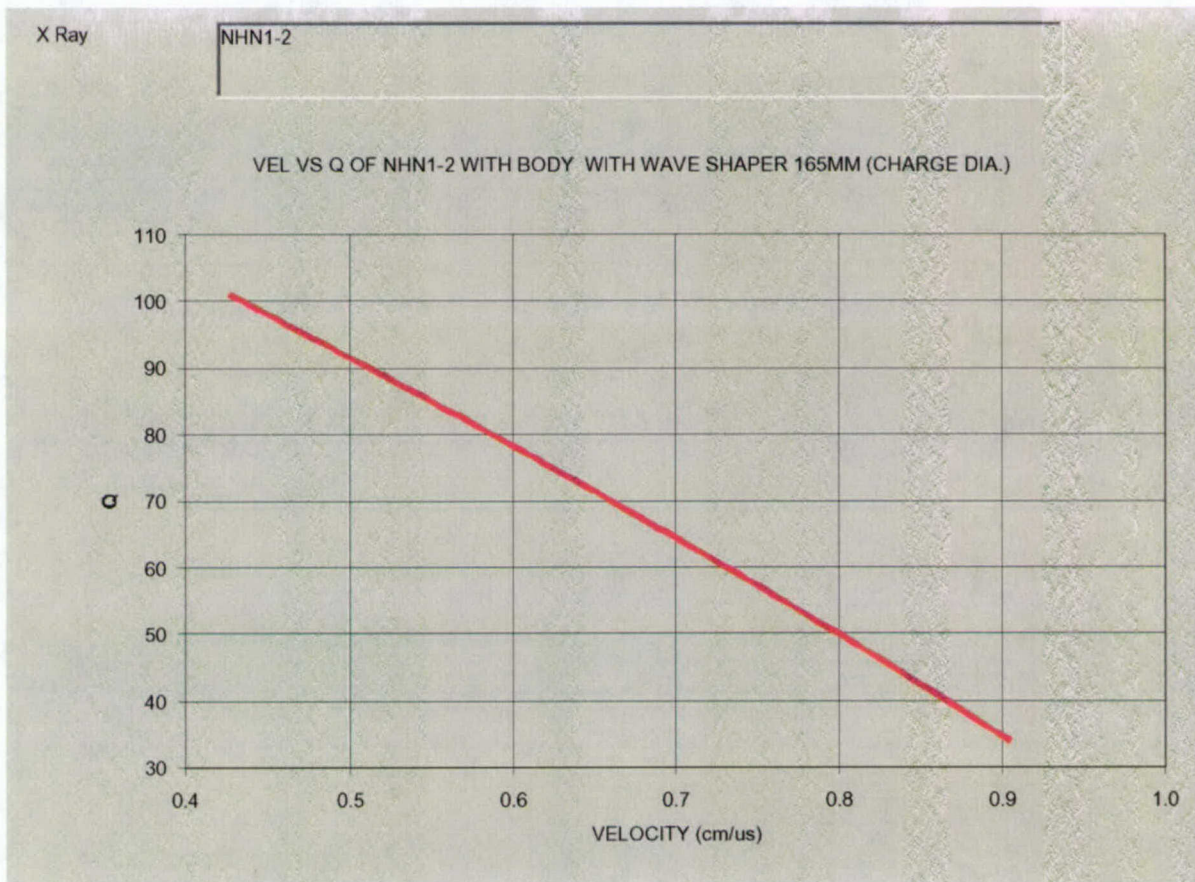


Figure 10  
Q versus velocity

### Maximum Jet Diameter and Average Jet Diameter

Jet diameter information provides a quick look on how well the jet performs in penetration and other calculations for jet properties (ref. 2).



$$\phi_{\max} = f_1(\bar{x}) - f_2(\bar{x})$$

where

$$\bar{x} = \frac{x_1 + x_5}{2}$$

The average jet diameter is estimated based on the assumption of the jet particle being a cylinder. Hence

$$\bar{\phi} = 2 \sqrt{\frac{Vol}{\pi L_p}}$$

where

$$L_p = x_5 - x_1$$

## DISCUSSIONS

Table 1 shows the tabulated form of the output from the code. The output lists all the jet parameters of interest. Note that particle 0 is the tip velocity, which is taken from the earlier films (films  $A_E$  and  $A_L$ ), and particle 1 uses this value. (In case only one A film is available, the tip velocity is taken from films A and B). Results from digitized data are compiled over the years for various liner materials and sizes. Tables 2 through 4 show the average Q values for copper, molybdenum, and tungsten, respectively. Although the average Q value varies with different configurations such as with a wave shaper, or with the body, or with different explosive, it is higher with copper than with molybdenum or tungsten liners.

Table 1  
Digitization output

Test Number NHN1-2  
 Density 10.49 g/cm<sup>3</sup>  
 The scale factor of A (EARLY) film: 0.9  
 The scale factor of A (LATE) film: 0.9  
 The scale factor of B film: 0.9  
 The scale factor of C film: 0.9  
 Last particle in film B: 58  
 First particle in film C: 44  
 Last particle in film C: 93  
 Early time A: 701.9  $\mu$ s (micro-seconds)  
 Late time A: 732  $\mu$ s  
 Time B: 701.9  $\mu$ s  
 Time C: 1001.5  $\mu$ s

---

Table 1  
(continued)

No.	Angle (deg)	Diameter (cm)		Velocity (cm/ $\mu$ s)	Acc. length (cm)	Acc. Mass (g)	Acc. Energy (KJ)	Breakup ( $\mu$ s)	Q
		Max.	Min.						
0	N/A**	N/A**	N/A**	0.903	N/A**	N/A**	N/A**	N/A**	N/A**
1	36	0.48	0.35	0.903	0.598	0.606	25.13	156.1	34.1
2	-59	0.16	0.11	0.897	1.232	0.685	27.89	160.7	35.0
3	-25	0.13	0.10	0.895	1.829	0.729	29.68	162.6	35.4
4	12	0.40	0.30	0.888	3.309	1.802	71.95	168.1	36.5
5	11	0.78	0.57	0.877	4.536	5.098	198.68	176.5	38.2
6	46	1.31	0.98	0.864	6.138	17.694	669.11	186.4	40.2
7	2	0.86	0.63	0.855	8.281	24.653	923.67	193.3	41.6
8	-49	0.47	0.34	0.845	9.457	25.775	963.68	201.7	43.3
9	30	0.25	0.19	0.842	10.974	26.225	979.62	203.9	43.7
10	-15	0.78	0.58	0.865	12.219	29.641	1,098.67	209.2	44.7
11	36	0.74	0.55	0.826	14.054	34.166	1,253.00	216.2	46.1
12	4	0.92	0.69	0.814	14.824	37.173	1,352.75	225.1	47.8
13	49	0.45	0.33	0.811	15.702	37.972	1,378.99	227.9	48.4
14	-47	0.54	0.39	0.807	16.713	39.258	1,420.91	230.7	48.9
15	52	0.52	0.38	0.804	17.594	40.319	1,455.17	233.5	49.5
16	-18	0.63	0.47	0.799	18.970	42.783	1,533.82	237.0	50.1
17	-14	0.70	0.51	0.795	20.002	44.989	1,603.56	240.0	50.7
18	3	0.71	0.53	0.788	21.332	48.085	1,699.58	246.0	51.8
19	-10	0.49	0.37	0.780	22.780	49.702	1,748.80	251.6	52.9
20	36	0.42	0.31	0.772	24.260	50.887	1,784.11	258.0	54.1
21	27	0.53	0.39	0.767	25.061	51.875	1,813.16	262.2	54.9
22	-12	0.47	0.34	0.763	26.239	53.018	1,846.43	264.9	55.4
23	60	0.25	0.19	0.758	26.879	53.199	1,851.63	268.6	56.1
24	42	0.61	0.45	0.758	27.913	54.902	1,900.54	269.1	56.2
25	-27	0.54	0.39	0.753	29.047	56.346	1,941.50	272.6	56.9
26	-30	0.49	0.36	0.748	30.829	58.278	1,995.54	276.7	57.6
27	1	0.70	0.53	0.745	31.391	59.601	2,032.26	279.1	58.1
28	-22	0.80	0.60	0.742	31.807	60.827	2,065.97	281.7	58.6
29	29	0.55	0.40	0.741	33.053	62.479	2,111.29	282.2	58.7
30	-1	0.47	0.35	0.734	35.610	65.002	2,179.32	287.3	59.6
31	4	0.47	0.35	0.727	36.107	65.512	2,192.83	292.7	60.6
32	4	0.50	0.37	0.726	37.720	67.324	2,240.60	293.6	60.8
33	-1	0.50	0.37	0.717	41.163	71.245	2,341.44	300.6	62.1
34	-1	0.50	0.36	0.705	42.636	72.852	2,381.40	309.9	63.8
35	0	0.29	0.21	0.703	43.180	73.054	2,386.39	311.8	64.1
36	6	0.49	0.36	0.701	45.525	75.563	2,448.03	313.3	64.4
37	7	0.44	0.32	0.694	46.828	76.675	2,474.76	319.0	65.5
38	31	0.47	0.35	0.689	48.101	77.957	2,505.20	322.3	66.1
39	2	0.43	0.32	0.687	49.734	79.319	2,537.32	324.3	66.4
40	18	0.46	0.34	0.683	51.016	80.527	2,565.52	327.0	66.9
41	-11	0.53	0.39	0.677	52.947	82.961	2,621.31	331.7	67.8
42	-58	0.22	0.17	0.671	53.373	83.062	2,623.57	336.6	68.6
43	-1	0.51	0.38	0.669	56.455	86.643	2,703.68	338.2	68.9
44	-5	0.68	0.50	0.660	56.974	87.698	2,726.63	345.3	70.2
45	0	0.51	0.38	0.656	60.145	91.401	2,806.41	347.8	70.7
46	10	0.50	0.37	0.647	61.443	92.864	2,837.05	355.0	71.9
47	13	0.34	0.25	0.649	62.088	93.203	2,844.18	353.5	71.7
48	-26	0.34	0.25	0.649	62.088	93.203	2,844.18	353.5	71.7
49	0	0.42	0.31	0.638	65.572	96.282	2,907.39	361.9	73.2
50	-7	0.45	0.33	0.636	67.920	98.451	2,951.28	363.5	73.5
51	15	0.46	0.34	0.633	69.544	99.966	2,981.63	366.1	73.9
52	-6	0.44	0.32	0.626	71.987	102.065	3,022.78	371.3	74.8

Table 1  
(continued)

No.	Angle (deg)	Diameter (cm)		Velocity (cm/ $\mu$ s)	Acc. length (cm)	Acc. Mass (g)	Acc. Energy (KJ)	Breakup ( $\mu$ s)	Q
		Max.	Min.						
53	-6	0.42	0.31	0.618	74.537	104.074	3,061.14	377.6	75.9
54	-1	0.42	0.31	0.614	77.726	106.604	3,108.89	380.5	76.4
55	3	0.38	0.28	0.610	80.513	108.423	3,142.69	384.2	77.1
56	4	0.42	0.31	0.606	81.578	109.256	3,157.96	387.2	77.6
57	3	0.38	0.28	0.602	84.490	111.165	3,192.59	389.8	78.1
58	-7	0.38	0.28	0.595	86.387	112.399	3,214.44	395.3	79.0
59	17	0.35	0.28	0.591	88.042	113.462	3,232.99	398.9	79.7
60	51	0.34	0.25	0.587	89.165	114.036	3,242.88	401.8	80.2
61	5	0.40	0.30	0.583	92.906	116.754	3,289.05	404.9	80.7
62	16	0.45	0.33	0.575	94.247	117.955	3,308.92	410.8	81.7
63	-1	0.47	0.35	0.573	95.768	119.450	3,333.42	413.0	82.1
64	3	0.43	0.31	0.568	97.667	120.999	3,358.38	416.7	82.7
65	0	0.51	0.37	0.561	100.305	124.030	3,406.15	421.6	83.6
66	-10	0.50	0.37	0.556	102.216	126.165	3,439.17	425.7	84.3
67	-10	0.42	0.31	0.552	103.276	126.993	3,451.78	429.0	84.9
68	7	0.41	0.30	0.550	104.515	127.939	3,466.07	430.6	85.1
69	8	0.10	0.30	0.546	106.987	129.752	3,493.05	433.9	85.7
70	6	0.47	0.31	0.538	108.972	129.752	3,493.05	433.9	85.7
71	6	0.41	0.30	0.536	110.726	132.965	3,539.50	441.0	86.9
72	-6	0.47	0.34	0.529	112.052	134.253	3,557.54	446.5	87.8
73	-20	0.39	0.29	0.527	113.183	135.016	3,568.11	448.6	88.2
74	-1	0.47	0.34	0.525	114.689	136.489	3,588.39	450.1	88.4
75	6	0.49	0.36	0.522	116.621	138.522	3,616.05	452.5	88.8
76	-3	0.40	0.30	0.517	118.164	139.630	3,630.89	455.8	89.4
77	-1	0.50	0.37	0.511	122.252	144.137	3,689.80	460.5	90.2
78	3	0.44	0.32	0.501	124.719	146.253	3,716.37	468.4	91.5
79	-2	0.49	0.36	0.494	127.386	149.029	3,750.30	473.6	92.4
80	-7	0.53	0.39	0.489	129.417	151.522	3,780.09	478.0	93.1
81	-8	0.46	0.35	0.482	131.712	153.733	3,805.77	483.3	94.0
82	-21	0.60	0.44	0.477	133.712	156.895	3,841.77	487.0	97.6
83	1	0.49	0.36	0.471	136.606	159.960	3,875.71	492.1	95.5
84	1	0.45	0.33	0.467	139.521	162.590	3,904.41	494.8	95.9
85	1	0.63	0.46	0.461	141.477	165.972	3,940.37	499.4	96.7
86	-35	0.49	0.36	0.457	142.714	167.287	3,954.10	502.8	97.2
87	-7	0.59	0.44	0.454	145.185	171.186	3,997.28	505.0	97.6
88	-8	0.59	0.43	0.450	146.712	173.529	4,018.06	507.7	98.0
89	-18	0.44	0.33	0.446	148.225	174.850	4,031.22	510.8	98.6
90	-6	0.59	0.44	0.444	150.465	178.394	4,066.14	512.9	98.6
91	-5	0.92	0.68	0.438	154.041	191.917	4,196.05	517.2	99.6
92	6	0.20	0.15	0.434	154.673	192.031	4,197.13	520.5	100.1
93	2	0.94	0.70	0.428	161.019	217.844	4,433.60	525.2	100.9

\*\* Tip velocity is based on earlier times on film A.

Table 1  
(continued)

Test Number NHN1-2  
Last particle of B is 58  
First particle of C is 44  
Last particle of C is 93

-----  
Coefficient VEL (cm/us) and Position of B (in)  
where  $VEL = b_0 + b_1 * x$   
 $b_0 = 1.004$   
 $b_1 = -0.005$

Coefficient VEL (cm/us) and Position of C (in)  
where  $VEL = b_0 + b_1 * x + b_2 * x^2$   
 $b_0 = 0.664$   
 $b_1 = -0.003$   
 $b_2 = 0.000$   
 $R^2 = 0.998$

Coefficient Acc Length (cm) and VEL (cm/us)  
where  $Acc\ Length = b_0 + b_1 * VEL + b_2 * VEL^2$   
 $b_0 = 456.428$   
 $b_1 = -857.592$   
 $b_2 = 388.310$   
 $R^2 = 0.998$

$t_{break} = 857.592 + -776.62 * VEL$

Coefficient Acc Mass (gram) and VEL (cm/us)  
where  $Acc\ Mass = b_0 + b_1 * VEL + b_2 * VEL^2$   
 $b_0 = 400.110$   
 $b_1 = -571.148$   
 $b_2 = 149.635$   
 $R^2 = 0.989$   
 $d(Acc\ Mass)/dVEL = 299.27 * VEL + -571.148$

Breakup time = 338.85us

Qave = 64.36

Table 2  
Average  $\bar{Q}$  values for copper lined devices

X-ray no.	Liner	Explosive	Tip velocity (cm/ $\mu$ s)	$\bar{Q}$
215	copper	LX-14	0.9	67
216	copper	LX-14	0.903	66
236	copper	Octol 70/30	0.85	60
237	copper	Octol 70/30	0.852	57
239	copper	Octol 70/30	0.858	74
290	copper	Octol 70/30	0.84	64
291	copper	Octol 70/30	0.841	76
292	copper	Octol 70/30	0.849	70
293	copper	TNAZ	0.887	68
312	copper	Octol 70/30	0.427	53
313	copper	Octol 70/30	0.296	54
315	copper	LX-14	0.912	64
316	copper	LX-14	0.894	67
317	copper	LX-14	0.882	70
318	copper	LX-14	0.905	65
319	copper	Octol 70/30	0.851	70
CLX2-18	copper	LX-14	1.027	72
BL1-50.2	copper	LX-19	1.008	76
326	copper	TNAZ 99.1	0.846	74
327	copper	LX-14	0.968	76
328	copper	TNAZ 99.1	0.872	71
329	copper	TNAZ 98.2	0.858	69
453	copper	LX-14	0.861	71
482	copper	LX-14	1.016	65
473	copper	LX-14	0.885	52
450	copper	LX-14	0.874	70
506	copper	LX-14	0.888	69
461	copper	LX-14	0.863	71
NHC-3-2	copper	LX-14	1.065	85
4-903	copper	LX-14	0.864	62
4-904	copper	PAX-12	0.91	73
4-905	copper	LX-14	0.947	67
NHC5-1	copper	PAX-12	1.075	62
5-031	copper	LX-14	0.984	68
4-744	copper	PAX-3	0.861	69
4-746	copper	PAX-3	0.725	64
RT04-079	copper	LX-14	0.696	55
6-566	copper	LX-14	0.872	54
NHN2-1	copper	PBXN-9	1.092	63

average  $\bar{Q}$

66.7

Table 3  
Average  $\bar{Q}$  values for molybdenum lined devices

X-ray no.	Liner	Explosive	Tip velocity (cm/ $\mu$ s)	$\bar{Q}$
M2-T2	molybdenum	PAX-2A	1.162	52
M2A1-16	molybdenum	PAX-2A	1.163	46
MC1-1	molybdenum	LX-14	1.135	58
NHM6-10	molybdenum	LX-14	1.212	42
NHM6-19	molybdenum	LX-14	1.122	40
RT04-077	molybdenum	LX-14	0.705	37
K charge	molybdenum	PBX-N9	1.105	56

average  $\bar{Q}$  47.3

Table 4  
Average  $\bar{Q}$  values for tungsten lined devices

X-ray no.	Liner	Explosive	Tip velocity (cm/ $\mu$ s)	$\bar{Q}$
188	Tungsten	Octol 70/30	0.849	41
238	Tungsten	Octol 70/30	0.933	41
241	Tungsten	Octol 70/30	0.912	41

average  $\bar{Q}$  41

Tables 5 through 7 show the average scaled breakup times for copper, molybdenum, and tungsten, respectively. As expected, the average  $t_b/D$  for copper devices is the highest among the three metals presented in this report. The results showed that copper is the most ductile material among the three metals presented here.

Table 5  
Average  $t_b/D$  values for copper lined devices

X-ray no.	Liner	Explosive	Tip velocity (cm/ $\mu$ s)	$t_b$ , breakup	D, charge diameter	$t_b/D$
215	Copper	LX-14	0.9	154	81	1.90
216	Copper	LX-14	0.903	150	81	1.85
236	Copper	Octol 70/30	0.85	155	81	1.91
237	Copper	Octol 70/30	0.852	149	81	1.84
239	Copper	Octol 70/30	0.858	184	81	2.27
290	copper	Octol 70/30	0.84	164	81	2.02
291	copper	Octol 70/30	0.841	193	81	2.38
292	copper	Octol 70/30	0.849	165	81	2.04
293	copper	TNAZ	0.887	165	81	2.04
312	copper	Octol 70/30	0.427	271	81	3.35
313	copper	Octol 70/30	0.296	333	81	4.11
315	copper	LX-14	0.912	179	81	2.21
316	copper	LX-14	0.894	180	81	2.22
317	copper	LX-14	0.882	196	81	2.42
318	copper	LX-14	0.905	175	81	2.16
319	copper	Octol 70/30	0.851	184	81	2.27

Table 5  
(continued)

X-ray no.	Liner	Explosive	Tip velocity (cm/ $\mu$ s)	tb, breakup	D, charge diameter	tb/D
CLX2-18	copper	LX-14	1.027	235	123	1.81
BL1-50.2	copper	LX-19	1.008	233	123	1.79
326	copper	TNAZ 99.1	0.846	194	81	2.40
327	copper	LX-14	0.968	185	81	2.28
328	copper	TNAZ 99.1	0.872	183	81	2.26
329	copper	TNAZ 98.2	0.858	175	81	2.16
453	copper	LX-14	0.861	178	81	2.20
482	copper	LX-14	1.016	160	81	1.98
473	copper	LX-14	0.885	138	81	1.70
450	copper	LX-14	0.874	170	81	2.10
506	copper	LX-14	0.888	176	81	2.17
461	copper	LX-14	0.863	183	81	2.26
NHC-3-2	copper	LX-14	1.065	235	123	1.91
4-903	copper	LX-14	0.864	162.5	81	2.01
4-904	copper	PAX-12	0.91	195	81	2.41
4-905	copper	LX-14	0.947	174	81	2.15
NHC5-1	copper	PAX-12	1.075	260	146	1.78
5-031	copper	LX-14	0.984	169	81	2.09
4-744	copper	PAX-3	0.861	154	81	1.90
4-746	copper	PAX-3	0.725	159	81	1.96
RT04-079	copper	LX-14	0.696	248	109	2.28
6-566	copper	lx-14	0.872	121.1	81	1.50
NHN2-1	copper	PBX-N9	1.092	276.1	165	1.67
				avg tb/D		2.15

Table 6  
Average  $t_b$  /D values for molybdenum lined devices

X-ray no.	Liner	Explosive	Tip Vel (cm/ $\mu$ s)	$t_b$ , breakup time ( $\mu$ s)	D, charge diameter (mm)	tb/D
90	molybdenum	Octol 70/30	1.145	87	73	1.19
95	molybdenum	Octol 70/30	1.165	101	73	1.38
149	molybdenum	Octol 70/30	1.163	107	73	1.47
167	molybdenum	Octol 70/30	1.088	122	73	1.67
172	molybdenum	Octol 70/30	1.183	91	73	1.25
174	molybdenum	Octol 70/30	1.125	117	73	1.60
M2-T2	molybdenum	PAX-2A	1.162	167	123	1.36
M2A1-16	molybdenum	PAX-2A	1.163	142	123	1.15
MC1-1	molybdenum	LX-14	1.135	199	123	1.62
NHM6-10	molybdenum	LX-14	1.212	118	98	1.20
NHM6-19	molybdenum	LX-14	1.122	108	98	1.10
RT04-077	molybdenum	LX-14	0.705	166	109	1.52
K charge	molybdenum	PBX-N9	1.105	223.5	165	1.35
				avg $t_b$ /D		1.37

Table 7  
Average  $t_b / D$  values for tungsten lined devices

X-ray no.	Liner	Explosive	Tip velocity (cm/ $\mu$ s)	$t_b$ , breakup time ( $\mu$ s)	D, charge diameter (mm)	$t_b/D$
188	tungsten	Octol 70/30	0.849	114	81	1.41
238	tungsten	Octol 70/30	0.933	115	81	1.42
241	tungsten	Octol 70/30	0.912	123	81	1.52
ave $t_b / D$						1.45

### ASSUMPTIONS

The density of the particles is assumed to be the same as that of the liner. It also assumes the cross sectional area of a jet particle is circular. The code takes into the virtual origin assumption in which all the jet mass particles are treated as coming from one point in space, each with a different velocity.

### COMPARISON TO 2-D HYDROCODE

Figure 11 shows the graphs of the accumulated mass versus velocity of the shaped charge digitization code and the 2-D CALE hydrocode of an 81-mm shaped charge warhead (without wave shaper, bare billet). The accumulated mass from the digitization showed that it matched the hydrocode simulation very well, especially at the tip region up to about 3 km/s.

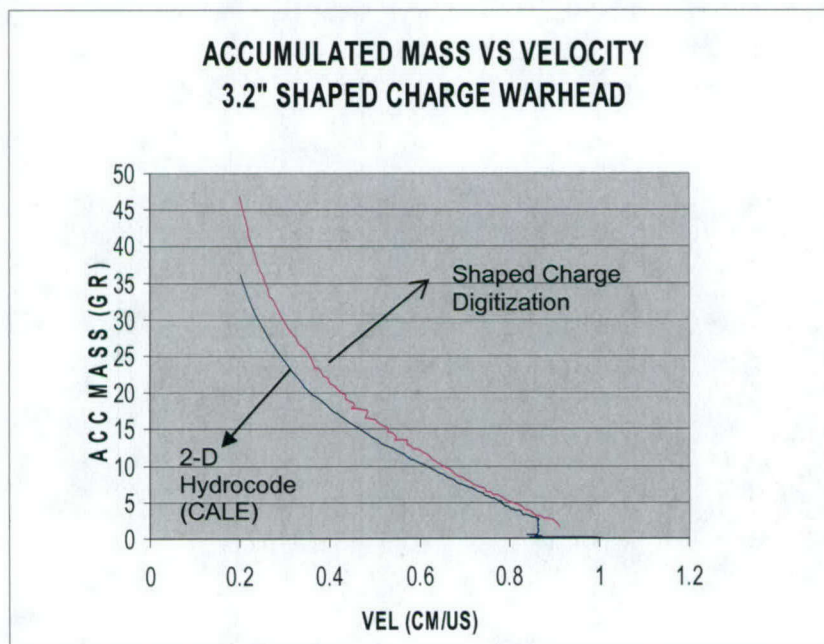


Figure 11  
Accumulated mass versus velocity from shaped charge digitization code and 2-D CALE hydrocode



## CONCLUSION

Flash radiograph shaped charge digitization program is a necessary tool for jet characterization of warhead performance. Jet parameters are calculated and quantified and subsequently used for penetration predictions. The results from the digitization reduction data is also used to check the results from the continuum modeling and help the optimization of the model during the warhead design of different liner contours, explosives and liner materials.

— APPENDIX  
OUTPUT FROM PROGRAM NO. 1, INPUT TO PROGRAM NO. 2











AP017792 4219 251  
 AP018041 4152 252  
 AP018189 4060 253  
 AP018065 3971 254  
 AP017882 3985 255  
 AP017690 4027 256  
 AP019888 4058 257  
 AP020304 4138 258  
 AP020787 4122 259  
 AP021037 4118 260  
 AP021394 4039 261  
 AP021175 3912 262  
 AP020718 3938 263  
 AP020354 3958 264  
 AP023096 4028 265  
 AP023305 4123 266  
 AP023441 4133 267  
 AP023551 4121 268  
 AP023740 4019 269  
 AP023579 3932 270  
 AP023444 3919 271  
 AP023265 3955 272  
 AP023733 3935 273  
 AP023808 3982 274  
 AP023864 3999 275  
 AP023921 3993 276  
 AP023971 3936 277  
 AP023906 3870 278  
 AP023856 3876 279  
 AP023813 3893 280  
 AP024258 3904 281  
 AP024506 4047 282  
 AP024800 4050 283  
 AP025002 4075 284  
 AP025278 4016 285  
 AP025143 3900 286  
 AP024841 3882 287  
 AP024614 3858 288  
 AP026250 3914 289  
 AP026436 4022 290  
 AP026571 4038 291  
 AP026712 4034 292  
 AP026816 3980 293  
 AP026725 3898 294  
 AP026624 3871 295  
 AP026507 3851 296  
 AP027400 3754 297  
 AP027502 3919 298  
 AP027615 3980 299  
 AP027740 4043 300

part B = 32  
 part B = 32  
 part B = 32  
 part B = 32  
 part B = 32  
 part B = 32  
 part B = 33  
 part B = 33  
 part B = 33  
 part B = 33  
 part B = 33  
 part B = 33  
 part B = 33  
 part B = 33  
 part B = 33  
 part B = 34  
 part B = 34  
 part B = 34  
 part B = 34  
 part B = 34  
 part B = 34  
 part B = 34  
 part B = 34  
 part B = 34  
 part B = 34  
 part B = 35  
 part B = 35  
 part B = 35  
 part B = 35  
 part B = 35  
 part B = 35  
 part B = 35  
 part B = 35  
 part B = 35  
 part B = 36  
 part B = 36  
 part B = 36  
 part B = 36  
 part B = 36  
 part B = 36  
 part B = 36  
 part B = 36  
 part B = 36  
 part B = 37  
 part B = 37  
 part B = 37  
 part B = 37  
 part B = 37  
 part B = 37  
 part B = 37  
 part B = 37  
 part B = 37  
 part B = 37  
 part B = 38  
 part B = 38  
 part B = 38  
 part B = 38

AP0 680811600AP05522911575  
 AP0 680811600AP05522911575  
 AP0 680811600AP05522911575  
 AP0 680811600AP05522911575  
 AP0 680811600AP05522911575  
 AP0 680811600AP05522911575  
 AP0 680811600AP05522911575  
 AP0 680811600AP05522911575  
 AP0 680811600AP05522911575  
 AP0 680811600AP05522911575  
 AP0 680811600AP05522911575  
 AP0 680811600AP05522911575  
 AP0 680811600AP05522911575  
 AP0 680811600AP05522911575  
 AP0 680811600AP05522911575  
 AP0 680811600AP05522911575  
 AP0 680811600AP05522911575  
 AP0 680811600AP05522911575  
 AP0 680811600AP05522911575  
 AP0 680811600AP05522911575  
 AP0 680811600AP05522911575  
 AP0 680811600AP05522911575  
 AP0 680811600AP05522911575  
 AP0 680811600AP05522911575  
 AP0 680811600AP05522911575  
 AP0 680811600AP05522911575  
 AP0 680811600AP05522911575  
 AP0 680811600AP05522911575  
 AP0 680811600AP05522911575  
 AP0 680811600AP05522911575  
 AP0 680811600AP05522911575  
 AP0 680811600AP05522911575  
 AP0 680811600AP05522911575  
 AP0 680811600AP05522911575  
 AP0 680811600AP05522911575  
 AP0 680811600AP05522911575  
 AP0 680811600AP05522911575  
 AP0 680811600AP05522911575  
 AP0 680811600AP05522911575  
 AP0 680811600AP05522911575  
 AP0 680811600AP05522911575  
 AP0 680811600AP05522911575  
 AP0 680811600AP05522911575  
 AP0 680811600AP05522911575























AP044629 7020 391  
AP044553 7032 392  
AP047119 6709 393  
AP047732 6842 394  
AP048512 6825 395  
AP049383 6960 396  
AP049893 6814 397  
AP049402 6531 398  
AP048858 6456 399  
AP048160 6572 400

part C = 92  
part C = 92  
part C = 93  
part C = 93  
part C = 93  
part C = 93  
part C = 93  
part C = 93  
part C = 93  
part C = 93

AP0 679511415AP05525811545  
AP0 679511415AP05525811545  
AP0 679511415AP05525811545  
AP0 679511415AP05525811545  
AP0 679511415AP05525811545  
AP0 679511415AP05525811545  
AP0 679511415AP05525811545  
AP0 679511415AP05525811545  
AP0 679511415AP05525811545  
AP0 679511415AP05525811545

AP020864 4814 1  
AP0 897116986 2

part A = 1  
part A = 2

AP0 679511415AP05525811545  
AP0 679511415AP05525811545

## REFERENCES

1. Chou, P.C.; Carleone, J.; and Walters, W.P.; "The Virtual Origin Approximation In Hemispherical Charges and Shaped Charges", Contract Report ARBRL-CR-00460, Dyna East Corp., PA, July 1981.
2. Pearson, J; Baker, E.L.; Orosz, J.P; Pham, J.P; Vuong, T.H; and Daniels, A.S., "New Data on Copper Lined and Other Shaped Charge Devices Providing Confirmation of The Walsh Jet Break Up Theory," Technical Report ARWEC-TR-03013, U.S. Army Armament Research, Development and Engineering Center, Picatinny, New Jersey, May 2004.
3. Vuong, T. H., Private Communication, July 2005.

## DISTRIBUTION LIST

U.S. Army ARDEC  
ATTN: AMSRD-AAR-EMK  
      AMSRD-AAR-GC  
      AMSRD-AAR-AEE-W (12)  
Picatinny, NJ 07806-5000

Defense Technical Information Center (DTIC)  
ATTN: Accessions Division  
8725 John J. Kingman Road, Ste 0944  
Fort Belvoir, VA 22060-6218

Commander  
Soldier and Biological/Chemical Command  
ATTN: AMSSB-CII, Library  
Aberdeen Proving Ground, MD 21010-5423

Director  
U.S. Army Research Laboratory  
ATTN: AMSRL-CI-LP, Technical Library  
Bldg 4600  
Aberdeen Proving Ground, MD 21005-5066

Chief  
Benet Weapons Laboratory, CCAC  
Armament Research, Development and Engineering Center  
U.S. Army Research, Development and Engineering Command  
ATTN: AMSRD-AAR-AEW  
Watervliet, NY 12189-5000

Director  
U.S. Army TRADOC Analysis Center-WSMR  
ATTN: ATRC-WSS-R  
White Sands Missile Range, NM 88002

Chemical Propulsion Information Agency For contractor releasable report,  
ATTN: Accessions unclassified and classified  
10630 Little Patuxent Parkway, Suite 202  
Columbia, MD 21044-3204

GIDEP Operations Center  
P.O. Box 8000  
Corona, CA 91718-8000